Journal of Catalysis xxx (2016) xxx–xxx

Contents lists available at ScienceDirect

Journal of Catalysis

journal homepage: www.elsevier.com/locate/jcat

Catalytic routes and oxidation mechanisms in photoreforming of polyols

Kai E. Sanwald [a], Tobias F. Berto [a], Wolfgang Eisenreich [a], Oliver Y. Gutiérrez [a,*], Johannes A. Lercher [a,b,*]

[a] TU München, Department of Chemistry and Catalysis Research Center, Lichtenbergstrasse 4, D-85747 Garching, Germany
[b] Pacific Northwest National Laboratory, Institute for Integrated Catalysis, P.O. Box 999, Richland, WA, USA

ARTICLE INFO

Article history:
Received 20 July 2016
Revised 19 August 2016
Accepted 21 August 2016
Available online xxxx

Keywords:
Photocatalysis
TiO_2
H_2 production
Photoreforming
Glycerol
Polyols
Oxidation mechanism

ABSTRACT

Photocatalytic reforming of biomass-derived oxygenates leads to H_2 generation and evolution of CO_2 *via* parallel formation of organic intermediates through anodic oxidations on a Rh/TiO_2 photocatalyst. The reaction pathways and kinetics in the photoreforming of C_3–C_6 polyols were explored. Polyols are converted *via* direct and indirect hole transfer pathways resulting in (i) oxidative rupture of C–C bonds, (ii) oxidation to α-oxygen functionalized aldoses and ketoses (carbonyl group formation) and (iii) light-driven dehydration. Direct hole transfer to chemisorbed oxygenates on terminal Ti(IV)-OH groups, generating alkoxy-radicals that undergo ß-C–C-cleavage, is proposed for the oxidative C–C rupture. Carbonyl group formation and dehydration are attributed to indirect hole transfer at surface lattice oxygen sites [Ti···O···Ti] followed by the generation of carbon-centered radicals. Polyol chain length impacts the contribution of the oxidation mechanisms favoring the C–C bond cleavage (internal preferred over terminal) as the dominant pathway with higher polyol carbon number.

1. Introduction

Photocatalytic H_2 generation from bio-derived oxygenates ('photoreforming') is a desired pathway for the production of a chemical energy carrier utilizing solar energy as it lowers the energy requirements compared to water cleavage [1–5]. Aqueous glycerol, an abundant by-product from triglyceride transesterification, and polyol-containing wastewaters, e.g. from industry or catalytic upgrading conceptually, could be suitable feedstocks for photoreforming [1–4,6]. Thereby valorization and/or purification of those resources are coupled to the production of H_2. Photoreforming benefits from a narrow energetic separation of the two redox half-reactions ($E^0(H^+/H_2) = 0$ V; e.g. for glycerol photoreforming $E^0(CO_2/C_3H_8O_3) = -0.004$ V vs. NHE [7]), which provides a large overpotential at the anode facilitating cathodic H_2 evolution. Moreover, compared to overall water splitting, substitution of the oxygen evolution reaction for anodic oxygenate oxidation to CO_2 eliminates the need of separation and the back-reaction of H_2 and O_2 [8].

While the electron-hole recombination and charge carrier transport to the surface and their relation to physicochemical properties of the photocatalyst have been explored with great depth [9–12], the role of the chemically coupled reactions have been hardly explored mechanistically and kinetically. In such reactions, the co-catalyst decorated semiconductor acts as coupled micro-electrochemical cell [13–15]. Anodic half-reactions are thought to occur on the semiconductor surface as a consequence of interfacial transfer of photogenerated holes through either direct transfer to the oxygenate or *via* an indirect mechanism, e.g. mediated by ·O(H)-radicals [6,16,17]. The co-catalyst serves as cathode, electron trap, and, thus, H_2 evolution site and does not participate in the anodic half-reactions [18,19]. Yet, H_2-evolution and thus oxygenate degradation rates (due to charge balance) are influenced by co-catalyst nature [7], loading and particle size [7,20] as well as its composition and morphology [21,22]. The co-catalyst could even aid the suppression of surface back-reactions at the cathode [8,23]. These factors provide essential means for optimization of the efficiency of electron transfer at the semiconductor/co-catalyst interface.

It is established that H_2-evolution rates over TiO_2-based photocatalysts depend on oxygenate nature and coverage [3,7,24–28]. However, there is ambiguity in the anodic pathways and mechanisms toward full oxidation to CO_2. Initial anodic transformations of polyols over metal/metal oxide loaded TiO_2 were proposed to result in the formation of the corresponding aldehydes, which undergo either decarbonylation followed by water-gas shift [17] or cleavage of formic acid [19]. Oxidation to carboxylic acids that decarboxylate [6,16] or initial polyol dehydration to compounds with non-functionalized carbon atoms [17] was also suggested

* Corresponding authors at: TU München, Department of Chemistry and Catalysis Research Center, Lichtenbergstrasse 4, D-85747 Garching, Germany (J.A. Lercher). Fax: +49 89 28913544.
E-mail addresses: oliver.gutierrez@mytum.de (O.Y. Gutiérrez), johannes.lercher@ch.tum.de (J.A. Lercher).

http://dx.doi.org/10.1016/j.jcat.2016.08.009
0021-9517/

prior to C–C-cleavage. On the other hand, photoreforming of linear aldehydes was reported to involve sequential cleavage of formic acid to form the C_1-deficient aldehyde in a single reaction pathway [19,29].

During aerobic photooxidation of oxygenates, multiple reaction pathways were accounted for by a two-site model for direct and indirect mechanisms [30–32]. Holes trapped at surface lattice oxygen sites [Ti···O···Ti] abstract a H-atom from a C–H bond whereas direct hole transfer yields alkoxy radicals chemisorbed on terminal OH-groups. We hypothesize that under photoreforming conditions (anaerobic environment and hydrogen evolving) similar mechanisms operate, which determine the routes toward complete oxidation. We have shown in a preceding contribution that the anodic transformations of ethylene glycol during photoreforming may be rationalized on this basis [18]. We further propose that identical anodic transformations are followed across families of compounds. However, the impact of molecular polyol structure and associated surface adsorption complexes on the contribution of the different reaction pathways to the complete oxidation is largely unknown.

Here, we explore the mechanisms and kinetics of photoreforming of C_3–C_6 polyols on benchmark TiO_2 P 25 with Rh as co-catalyst. On the basis of quantitative analysis of gas- and liquid-phase species we establish general relationships between structural reactant functional groups, anodic reaction pathways and oxidation mechanisms. We provide rationalization of the impact of anodic surface chemistry on the photoreforming kinetics in terms of oxygenate conversion and associated H_2-evolution rates.

2. Experimental

A comprehensive list of compounds used during the study, and detailed experimental procedures regarding the characterization of the photocatalyst are compiled in the Supporting Information. Briefly, experiments are conducted over AEROXIDE® TiO_2 P 25 (referred to as TiO_2 hereafter), commonly employed as benchmark semiconductor, decorated with nanoparticulate Rh as a co-catalyst (1 wt.% loading, particle size 1.9 nm (±0.7 nm), dispersion 57%). Further physicochemical properties of the materials are described in the Supporting Information.

2.1. Photocatalyst preparation

The 1 wt.% Rh-decorated P 25 photocatalyst, hereafter referred to as Rh/TiO_2, was prepared *via* incipient wetness impregnation. TiO_2 P 25 was dried under a static air atmosphere at 473 K for 2 h prior to impregnation. Subsequently, the semiconductor was treated with appropriate amounts of an aqueous solution of $RhCl_3 \cdot xH_2O$ in ultrapure water. The resulting precursor was kept in synthetic air at 383 K for 1 h (100 mL min^{-1}, 5 K min^{-1}) and heated to 623 K (100 mL min^{-1}, 5 K min^{-1}) for 1 h. The material was allowed to cool to room temperature before treatment in H_2 at 623 K (100 mL min^{-1}, 5 K min^{-1}) for 1 h. A TiO_2 reference was prepared subjecting as-received TiO_2 P 25 to the same temperature and gas treatments described before.

2.2. Photocatalytic test

2.2.1. Photoreforming experiments

Kinetic experiments were performed in a Pyrex top-irradiation photo-reactor connected to a closed gas-circulation system [18]. The setup is equipped with facilities for *online* gas-analysis and liquid-phase sampling. Irradiation is provided by a 300 W Xe lamp with a cold mirror 1 (CM 1). A water filter with quartz windows closes the top of the photo-reactor. The photon flux within the reactor at water level is $8.08 \cdot 10^{17}$ s^{-1} ($\lambda < 390$ nm). Typically, 75 mg of photocatalyst were ultrasonically dispersed in 100 mL of a 20 mM aqueous reactant solution. The system was deaerated by four consecutive evacuations and Ar filling cycles. All reactions were carried out at 288 K and an Ar pressure of 1 bar.

Evolved gases during photocatalytic reactions were analyzed *online via* gas chromatography (Shimadzu, GC 2010 Plus) on a Chromosorb 101 and a Molsieve 5 Å column with a TCD, FID and a methanizer catalyst unit. Ar was used as a carrier gas.

Aliquots of the liquid-phase were manually taken at regular times from the photocatalyst suspension *via* a sample valve. The solid was separated by filtering through 0.2 μm nylon filters. Liquid-phase species were quantitatively analyzed by ^{1}H NMR spectroscopy. Additionally, high-performance liquid chromatography (HPLC) analysis was performed for photoreforming experiments with C_4–C_6 oxygenates.

Reactant conversions X_A were calculated according to $X_A(\%) = (1 - \frac{N_A(t)}{N_{A,0}}) \cdot 100$, where $N_A(t)$ is the time-dependent molar amount of reactant A and $N_{A,0}$ is the initial molar amount of reactant A, i.e. present at the beginning of the reaction.

2.2.2. ^{1}H NMR analysis

For quantitative ^{1}H NMR measurements reactor aliquots were mixed in a 1:1 volume ratio with an external standard that contained 20 mM 1,3,5-trihydroxybenzene in D_2O adjusted to pH 3 with DCl. ^{1}H NMR spectra with water signal suppression were recorded at 305 K using an Avance III HD 500 System (Bruker Biospin, Rheinstetten, Germany) with an UltraShield 500 MHz magnet (11.75 T) and a BBI 500 S2 probe head (5 mm, inverse ^{1}H/X with Z-gradient). The resonance frequency of ^{1}H was 500.13 MHz. The spectra were acquired using the one-dimensional NOESY sequence from the Bruker library "noesygppr1d" with presaturation of the residual water signal during the relaxation delay and the mixing time using spoil gradients. Longitudinal relaxation times (T1) were determined by the inversion recovery pulse method. Relaxation delay and acquisition time were set to 26 s and 4.1 s, respectively. The sum of the latter corresponds to at least three times T1 of the slowest relaxing ^{1}H-nucleus (formic acid) and ensures quantitative analysis. Typically, 64 or 128 scans, with 64 k data points were collected. An exponential window function with a line broadening of 0.2 Hz was applied prior to Fourier transformation and the spectra were manually phased, baseline corrected and integrated using Mestre-C 8.1.1 software package. Liquid-phase species were identified according to their chemical shifts (referenced to the internal standard, see SI-Table 1) and in comparison with spectra of commercial references recorded under identical conditions. Overlapping signals were deconvoluted using Lorentzian-Gaussian shape type fitting functions. Quantification was done on the basis of the integrated signal intensities which were further calibrated against prepared solutions of known concentration in order to account for signal damping due to the water-suppression in close proximity to the water resonance frequency.

2.2.3. ^{13}C NMR analysis

For ^{13}C NMR measurements, reactor aliquots were again mixed in a 1:1 volume ratio with D_2O adjusted to pH 3 with DCl. ^{13}C NMR spectra were recorded at 300 K using an Avance III 500 System (Bruker Biospin, Rheinstetten, Germany) with an UltraShield 500 MHz magnet (11.75 T) and a Cryo-QNP probe head (5 mm, direct ^{13}C/^{31}P/^{29}Si/^{19}F with Z-gradient). The resonance frequency of ^{13}C was 125.07 MHz. The spectra were acquired using the one-dimensional "zgpg" sequence from the Bruker library using waltz16 ^{1}H-decoupling and a 30° ^{13}C-pulse. Relaxation delay and acquisition time were set to 4 s and 1.2 s, respectively. Typically, 1024 scans with 64 k data points were collected. An exponential

Please cite this article in press as: K.E. Sanwald et al., Catalytic routes and oxidation mechanisms in photoreforming of polyols, J. Catal. (2016), http://dx.doi.org/10.1016/j.jcat.2016.08.009

window function with a line broadening of 1 Hz was applied prior to Fourier transformation and the spectra were manually phased, baseline corrected and integrated using Mestre-C 8.1.1 software package. Signals were assigned according to their chemical shifts in comparison with spectra of commercial references recorded under identical conditions.

2.2.4. HPLC analysis

Complementary HPLC analysis on an Agilent HP series 100 equipped with a refractive index (RI, 313 K) and a diode array ultraviolet (UV) detector was performed for quantification of erythritol, arabitol and sorbitol. Liquid-phase species were separated on an ion-exclusion column (Rezex ROA, Phenomenex) held at 343 K. 0.005 M H_2SO_4 was used as the mobile phase flowing at 0.5 mL min^{-1}. Reactor aliquots were mixed in a 4:1 volume ratio with an aqueous solution containing 1,3-propylene glycol as internal standard before injection. Integrated signal areas were calibrated against prepared solutions of known concentration.

Combined determination of gas- and liquid-phase concentrations of reaction products and intermediates allowed to quantitatively follow photoreforming kinetics with closed mass-balances.

3. Results and discussion

3.1. Kinetics of photoreforming of glycerol and C_3 intermediates

3.1.1. Glycerol photoreforming

Photoreforming of glycerol (Scheme 1) proceeded with continuous evolution of H_2 and CO_2 (1405 μmol and 366 μmol, respectively after 12 h reaction time) reaching a conversion of 39% after 12 h. The H_2-evolution rates declined over time from a maximum value of 143 μmol h^{-1} to about 95 μmol h^{-1} after 12 h (Fig. 1A). This decline is related to a first-order dependence on concentration (SI-Fig. 3, see kinetic model in Section 3.2 and Supporting Information). Chemical transformations were not observed in absence of illumination.

H_2/CO_2-ratios (Fig. 1B), which decreased throughout the reaction period, were above the theoretical ratio of 2.3 expected from Scheme 1 (ratio of 3.8 after 12 h). This observation indicates that full oxidation of glycerol to CO_2 occurs with the formation of organic intermediates in the liquid-phase. A list of molecular structures and overall reaction equations are furthermore given in SI-Table 3. Analysis of the aqueous-phase (Fig. 2) revealed that formaldehyde (613 μmol after 12 h) was generated as the major species linearly accumulating in solution with reaction time. The oxidation of formaldehyde is slow in the presence of other oxygenates during photoreforming due to its comparatively low apparent adsorption constant on TiO_2 [18].

Three C_3-species are formed from glycerol in low amounts: glyceraldehyde (GAD, 24 μmol after 12 h) and dihydroxyacetone (DHA, 45 μmol after 12 h) generated *via* two electron oxidation of a primary or secondary carbon atom of glycerol, respectively, as well as hydroxyacetone (HA, 5 μmol after 12 h) formally resulting from a light-driven dehydration. A steady-state concentration of GAD in solution is attained after 4 h indicating consumption of GAD by consecutive reactions. Similarly, the amount of DHA tended to level off with increasing reaction time while the concentration of HA increased gradually with reaction time. In addition to small amounts of formic acid (25 μmol after 12 h), three C_2-species, i.e. glycolaldehyde (275 μmol after 12 h), acetaldehyde (30 μmol after 12 h) (whose temporal profile is indicative of a secondary reaction product), and traces of acetic acid (2 μmol after 12 h) were detected. Interconversion and/or equilibration of GAD and DHA *via* keto-enol tautomerism was not observed under reaction conditions. We concluded that at least three parallel reaction pathways for glycerol oxidation exist, because three non-interconvertible C_3-products were observed (Scheme 2). Further analysis indicated that a fourth pathway exists yielding glycolaldehyde and formaldehyde directly from glycerol (Path 4, *vide infra*).

3.1.2. Path 1: Glyceraldehyde (GAD) photoreforming

Photoreforming of GAD yielded H_2 and CO_2 (1264 μmol and 387 μmol, respectively after 12 h) in the gas-phase. In contrast to

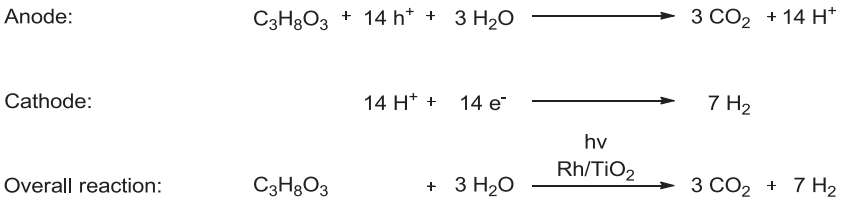

Scheme 1. Cathodic, anodic half-reactions and overall photoreforming reaction of glycerol.

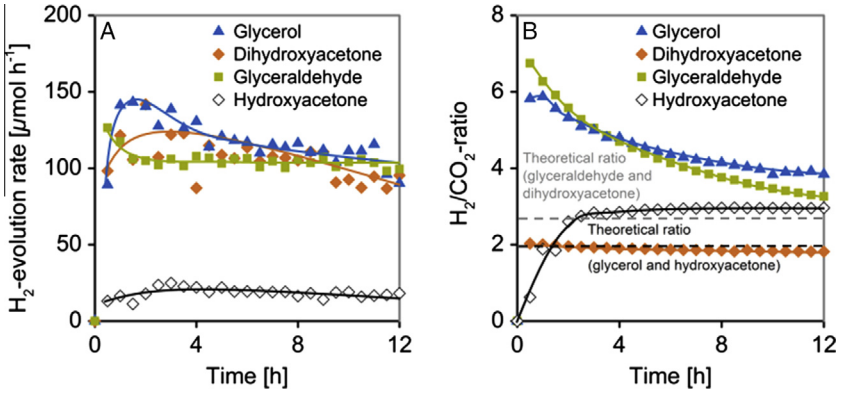

Fig. 1. (A) Course of H_2-evolution rates during photoreforming of C_3-oxygenates. (B) Course of H_2/CO_2-ratios. Curved lines are drawn as a guide to the eye. Dashed horizontal lines in (B) represent the stoichiometric ratios expected from the overall reaction equations. Reaction conditions: 75 mg photocatalyst, 100 mL aqueous oxygenate solution (20 mM), 288 K, 1 bar Ar, 300 W Xe-lamp (CM1).

Please cite this article in press as: K.E. Sanwald et al., Catalytic routes and oxidation mechanisms in photoreforming of polyols, J. Catal. (2016), http://dx.doi.org/10.1016/j.jcat.2016.08.009

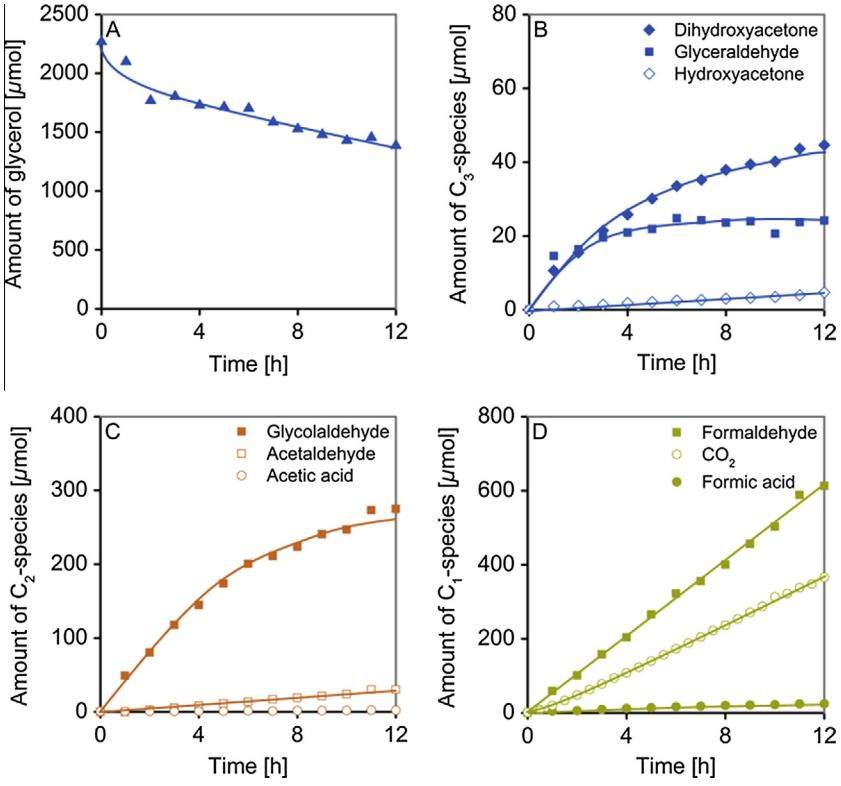

Fig. 2. Analysis of species generated in anodic half-reactions during glycerol photoreforming. (A) Course of the amount of glycerol. Quantities of different (B) C_3-, (C) C_2- and (D) C_1-species generated. Reaction conditions: 75 mg photocatalyst, 100 mL aqueous glycerol solution (20 mM), 288 K, 1 bar Ar, 300 W Xe-lamp (CM1).

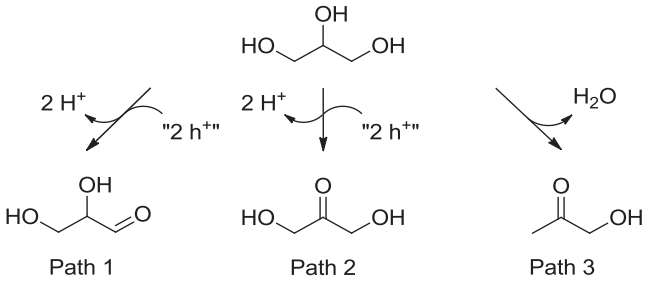

Scheme 2. Initial conceptual reaction pathways for glycerol photoreforming over Rh/TiO_2 on the basis of identification of three C_3-species generated in the liquid-phase.

glycerol photoreforming, H_2-evolution from GAD occurred with constant rate over time (Fig. 1A). Analysis of the liquid-phase species (Fig. 3) showed glycolaldehyde (614 µmol after 12 h) as the dominant species accompanied by formic acid (steady-state amount of 421 µmol after 12 h), small amounts of formaldehyde (158 µmol after 12 h) and traces of acetaldehyde and acetic acid (18 µmol and 7 µmol after 12 h, respectively). Oxidation of GAD did not yield glyceric acid as intermediate prior to C–C-scission as proposed in previous studies on photocatalytic conversion of glycerol [6,16,33] based on observations from electrocatalytic oxidation of glycerol and GAD [34–38].

The temporal profiles indicate that anodic conversion of GAD involves C–C-cleavage to form glycolaldehyde and a C_1-species.

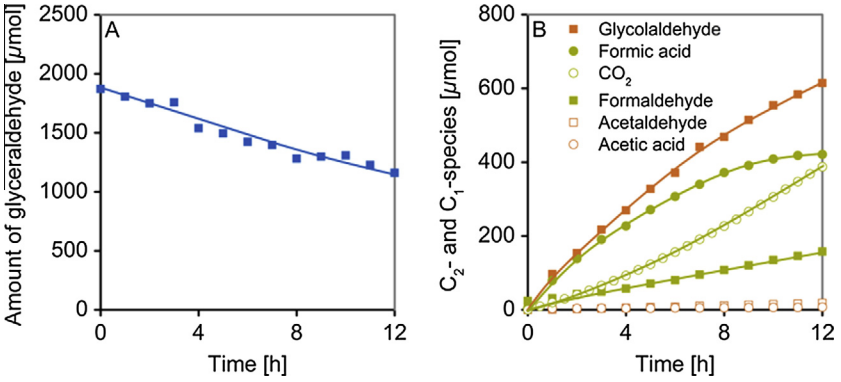

Fig. 3. Course of anodic reaction products formed during glyceraldehyde photoreforming. (A) Course of amount of glyceraldehyde. (B) Temporal profiles of C_2- and C_1-species generated. Reaction conditions: 75 mg photocatalyst, 100 mL aqueous glyceraldehyde solution (20 mM), 288 K, 1 bar Ar, 300 W Xe-lamp (CM1).

Please cite this article in press as: K.E. Sanwald et al., Catalytic routes and oxidation mechanisms in photoreforming of polyols, J. Catal. (2016), http://dx.doi.org/10.1016/j.jcat.2016.08.009

As the amounts of CO_2 and trace CO (4.4 μmol CO after 12 h) produced do not account for the amount of GAD converted (711 μmol after 12 h), the C_1 moiety cleaved from GAD must be contained in formic acid, which forms at equimolar concentrations than glycoladehyde at low reaction time. Subsequent photoreforming of glycoladehyde proceeds *via* a selective C–C bond cleavage yielding equimolar amounts of formic acid and formaldehyde [18,19]. As the apparent adsorption constants of both species differ by two orders of magnitude (see Chapter 3.2) consecutive oxidation of formic acid to CO_2 occurs more rapidly than conversion of formaldehyde to formic acid. Indeed, formaldehyde conversion is negligible under reaction conditions while CO_2 is generated from formic acid oxidation [18]. This supports our conclusion of the C–C bond cleavage of GAD proceeding *via* formation of formic acid and glycolaldehyde (see the Supporting Information, see also SI-Fig. 4). The reaction pathway for full anodic conversion of glycerol to CO_2 *via* GAD (Path 1), glycolaldehyde and the respective C_1-species is depicted in Scheme 3.

3.1.3. Path 2: Dihydroxyacetone (DHA) photoreforming

The ratio of the amounts of H_2 and CO_2 (1247 μmol and 686 μmol, respectively after 12 h) evolved determined for DHA photoreforming was close to two during the entire reaction (Fig. 1B), i.e., the ratio corresponding to the overall reaction equation (SI-Table 3). Along with formic acid (11 μmol after 12 h), the liquid-phase contained formaldehyde in quantities, which exceed the amount of DHA converted (1038 μmol and 656 μmol, respectively after 12 h) (Fig. 4). This indicates that more than one equivalent of formaldehyde was formed from DHA and consecutive oxidations. The H_2/CO_2 ratio and quantities of liquid-phase products indicate that DHA photoreforming proceeds *via* formation of two equivalents of formaldehyde and one equivalent of CO_2. Only small amounts of C_2-species, i.e. glycolaldehyde and glycolic acid (24 μmol and 2 μmol, respectively after 12 h), were present. During reforming of an equimolar mixture of DHA and glycolic acid, the latter was converted at much higher rates than the former (SI-Fig. 5), whereas formaldehyde and CO_2 were observed at concentrations similar to those observed during the reforming of DHA alone.

Thus, we conclude that the photoreforming of DHA proceeds *via* glycolic acid as C_2-intermediate in the first reaction step simultaneously generating one H_2-equivalent at the cathode (Scheme 4). Consecutively, glycolic acid undergoes fast oxidative decarboxylation to form second equivalents of formaldehyde and H_2 (Scheme 4).

Our reaction pathway studies are guided by the principle that stable organic species may be formed after two electron oxidation. In contrast, the formation of glycolaldehyde and formaldehyde from DHA requires the formation of a new C-H bond at the carbonyl carbon atom, which corresponds to a redox-neutral transformation, i.e., one electron oxidation of a primary carbon of DHA to form formaldehyde along with one electron reduction of the secondary carbon. Under photoreforming conditions, a redox-neutral transformation of this kind must be slow because the availability of electrons at the semiconductor surface is expected to be greatly limited in the presence of the co-catalyst acting as an electron trap. An alternative redox-neutral process would involve diffusion of a radical oxidant species to the metal, where the reduction step would occur competing with H_2-evolution. Thus, generation of glycolaldehyde as relevant C_2-intermediate in the reforming of DHA is considered a minor side reaction.

During photoreforming of the next higher homologous ketose of DHA (erythrulose, refer to SI-Figs. 6 and 7), also the characteristic H_2/CO_2-ratio of two was observed, while the corresponding C_3-intermediate acid could not be detected. Thus, in the photoreforming of linear ketoses intermediate C_{n-1} acid, if formed, rapidly reacts further yielding a C_{n-2} aldehyde as apparent primary product.

3.1.4. Path 3: Hydroxyacetone (HA) photoreforming

The amounts of H_2 and CO_2 (222 μmol and 57 μmol, respectively after 12 h) evolved during photoreforming of HA are about 80% lower than those from DHA, GAD, and glycerol. In general, H_2-evolution rates are lower for compounds carrying non-oxygen-functionalized carbons compared to their counterparts with maximum number of oxygen-functionalities. In particular, α-oxygen functionalization is required for efficient hole transfer [18,24,25,39]. Note that the amounts of H_2 obtained from photoreforming of 20 mM solutions of 1,2- and 1,3-propanediol (997 μmol and 447 μmol after 12 h, respectively) were lower than those from glycerol (1405 μmol after 12 h) under identical reaction conditions.

Liquid-phase analysis (Fig. 5) during HA photoreforming disclosed acetic acid as a main primary product and formaldehyde (99 μmol and 56 μmol, respectively, after 12 h). Formic acid is virtually absent (1 μmol after 12 h). Acetaldehyde, which is known to undergo slow consecutive oxidation to acetic acid, and hence to accumulate in liquid-phase [40,41], was not observed. This suggests that acetic acid was indeed formed as a primary product from HA. Consecutive oxidation of acetic acid may progress either to CO_2, or to CH_4 and CO_2 (Photo-Kolbe reaction) [18,42–44] suggested by the detection of CH_4 in the gas-phase (5 μmol CH_4 after 12 h). In line with the concluded decomposition of HA *via* acetic acid (associated to low H_2-evolution rates), considerably lower H_2-evolution rates from acetic acid/acetate solutions in comparison with C_1–C_3 alcohols and polyols have been obtained over noble metal decorated TiO_2 [25,44].

In analogy to DHA photoreforming, we conclude that formaldehyde is generated with acetic acid upon C–C scission of HA. The reaction pathway for glycerol photoreforming *via* intermediate formation of HA is represented in Scheme 5. HA contents during glycerol photoreforming were the smallest among the C_3-intermediates generated while the consecutive reforming reactions

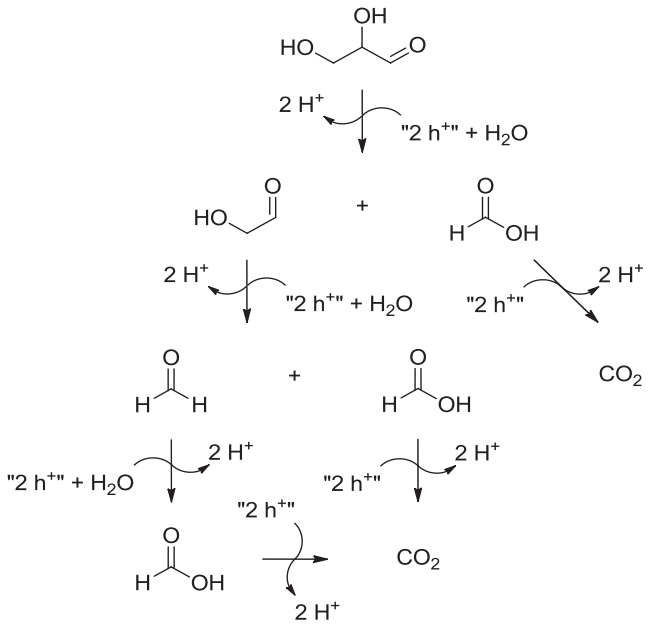

Scheme 3. Reaction pathway for photocatalytic reforming of glycerol (Path 1): Glycerol is oxidized to glyceraldehyde. Subsequent reaction steps involve sequential cleavage of formic acid through intermediate glycolaldehyde (C_{n-1} aldehyde) and formaldehyde (C_{n-2} aldehyde) toward full oxidation to CO_2.

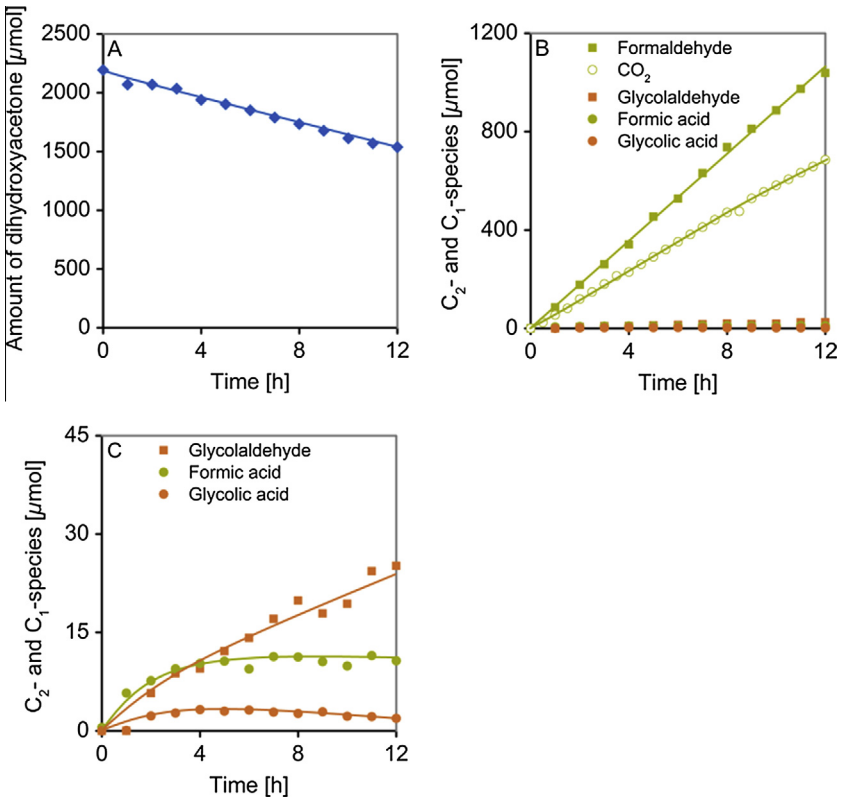

Fig. 4. Course of anodic reaction products formed during dihydroxyacetone photoreforming. (A) Course of amount of dihydroxyacetone. (B) Temporal profiles of C_2- and C_1-species generated. (C) Expanded view of (B) to show the reaction products generated in low amounts. Reaction conditions: 75 mg photocatalyst, 100 mL aqueous dihydroxyacetone solution (20 mM), 288 K, 1 bar Ar, 300 W Xe-lamp (CM1).

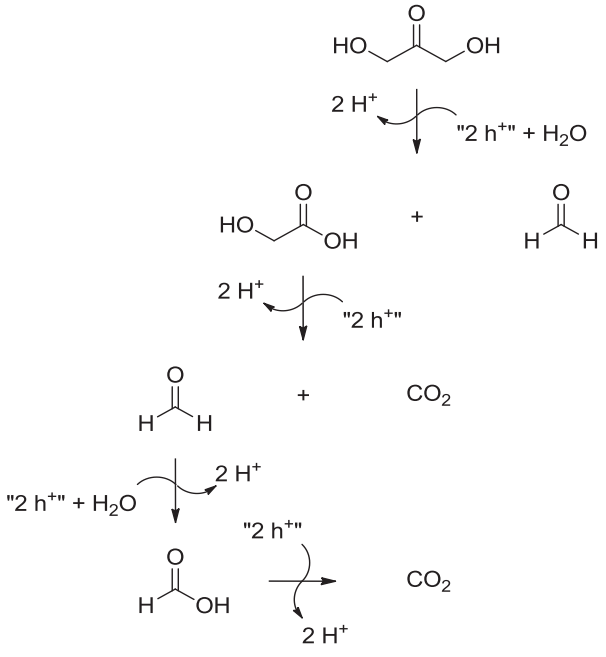

Scheme 4. Reaction pathway for photocatalytic reforming of glycerol (Path 2): Two electron oxidation of glycerol to form dihydroxyacetone. Consecutive dihydroxyacetone conversion via glycolic acid yields CO_2 and two equivalents of formaldehyde.

of HA are significantly slower compared to GAD and DHA. Thus, the light induced dehydration of glycerol to HA is a side-reaction.

3.2. Path 4: Direct oxidative C–C-cleavage of glycerol

Photoreforming of glycerol DHA, GAD, and HA showed different initial H_2-evolution rates under identical reaction conditions. However, the rates converge towards a maximum value of 200 µmol h^{-1} with increasing initial concentration in agreement with a Langmuir-type kinetics (SI-Fig. 8). This agrees also well with photocatalytic conversion of C_2-oxygenates over Rh/TiO_2 [18]. Assuming the intrinsic rate constants to be substrate independent, this indicates that photoreforming rates of oxygenates primarily depend on their apparent adsorption constants and associated surface coverages (under constant illumination conditions) irrespective of the nature of the charge carrier transfer mechanism. Hence, a model based on Langmuir adsorption applies to describe the kinetics of photoreforming of the studied oxygenates as quantitatively outlined in the Supporting Information.

Direct oxidative C–C-cleavage of glycerol to yield glycolaldehyde and formaldehyde, which had been proposed during aerobic conversion of glycerol over non-metallized TiO_2 P 25 [31], had to be included in the model (besides the parallel reaction pathways from glycerol that yield C_3 oxygenates) in order to achieve reasonable agreement with the experimental data. Evidence for this transformation is provided from the product distributions obtained for photoreforming of higher polyols and is discussed in Section 3.3.

Kinetic modeling confirmed a negligible contribution of HA formation from glycerol and successive oxidations (Path 3). In conclusion, we propose the reaction network depicted in Scheme 6 for glycerol photoreforming from gas-, liquid-phase analysis and kinetic modeling. Anodic glycerol conversion predominantly involves oxidative C–C-scission (61%) to yield glycolaldehyde and formaldehyde. Oxidations of primary and secondary carbons,

Please cite this article in press as: K.E. Sanwald et al., Catalytic routes and oxidation mechanisms in photoreforming of polyols, J. Catal. (2016), http://dx.doi.org/10.1016/j.jcat.2016.08.009

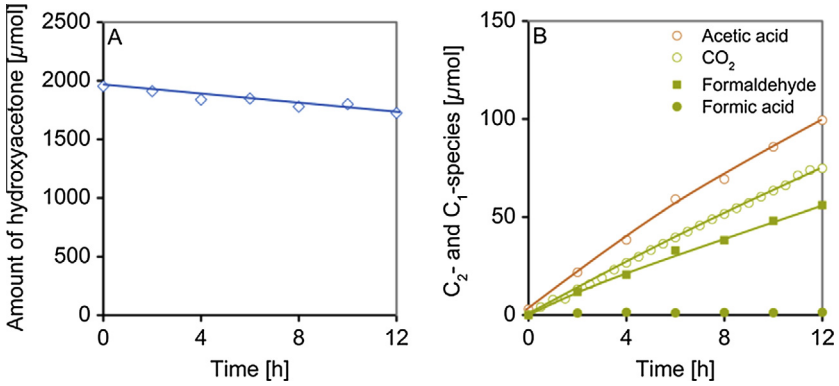

Fig. 5. Course of anodic reaction products formed during photoreforming of hydroxyacetone. (A) Course of amount of hydroxyacetone. (B) Temporal profiles of C_2- and C_1-species generated. Reaction conditions: 75 mg photocatalyst, 100 mL aqueous hydroxyacetone solution (20 mM), 288 K, 1 bar Ar, 300 W Xe-lamp (CM1).

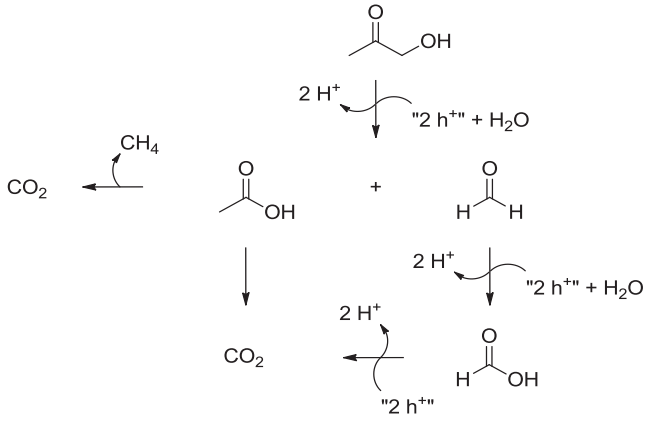

Scheme 5. Reaction pathway for photocatalytic reforming of glycerol (Path 3): Light-driven dehydration of glycerol to form hydroxyacetone. Consecutive oxidation of hydroxyacetone leads to the formation of acetic acid and formaldehyde intermediates toward full oxidation to CO_2.

which lead to the formation of GAD (26%) and DHA (13%), represent minor reaction channels. A comparison of experimental and fitted photoreforming kinetics of glycerol, GAD and DHA and the corresponding apparent adsorption constants of C_1–C_3 oxygenates are given in SI-Figs. 9–11 and SI-Table 4.

3.3. Photoreforming of C_4–C_6 polyols

The courses of the H_2-evolution rates during photoreforming of erythritol, arabitol and sorbitol (C_4, C_5, and C_6 polyols, respectively) are presented in Fig. 6. The 49% decline from initial H_2-evolution rates over 12 h of reaction time, particularly steep during the first 4 h for all three polyols, is more pronounced than for glycerol photoreforming (33%). The course of the evolution of intermediates and reaction products in the anodic half-reactions during sorbitol photoreforming is exemplarily depicted in Fig. 7 (corresponding data for erythritol and arabitol are found in SI-Figs. 12 and 13).

The product distributions in the photoreforming of erythritol, arabitol and sorbitol show common features. All shorter chain (C_{n-1}, C_{n-2}, etc.) aldoses with decreasing carbon number down to C_2 and formaldehyde were encountered during photoreforming of the corresponding C_n polyol. However, higher initial selectivities were obtained to C_{n-2} aldoses (being constant over time) compared to C_{n-1} aldoses and formaldeyde. Furthermore, glycolaldehyde is the major species in each case accumulating over time in liquid-phase, with the highest and almost constant selectivity with increasing reaction time (SI-Figs. 14–16). Larger amounts of glycolaldehyde were produced at similar amounts of H_2 generated with increasing polyol carbon number (SI-Table 5). These observations indicate that glycolaldehyde is not formed as a result of a reaction cascade, but as a primary product from the polyols. Thus, initial

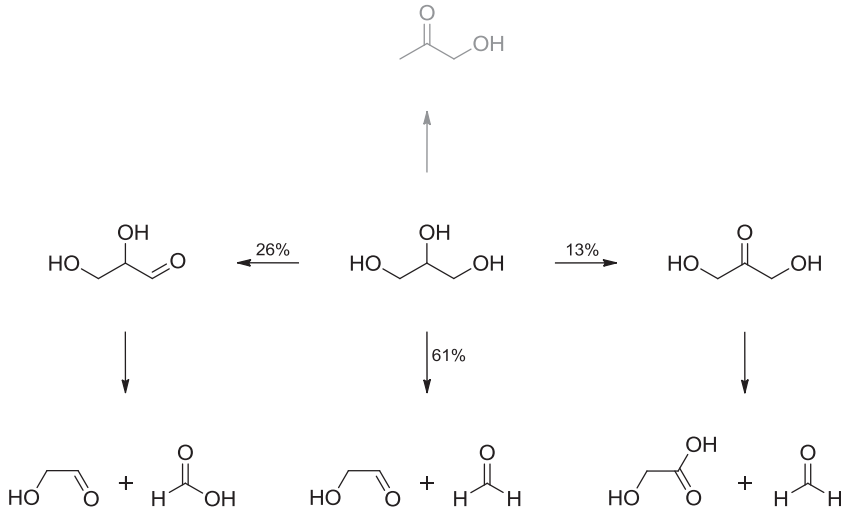

Scheme 6. Reaction network for photocatalytic reforming of glycerol. Initial anodic glycerol transformation involves four reaction pathways. C–C-cleavage to form glycolaldehyde and formaldehyde occurs primarily over formation of carbonyl groups to produce glyceraldehyde or dihydroxyacetone. Light-driven dehydration to hydroxyacetone constitutes a side reaction.

Please cite this article in press as: K.E. Sanwald et al., Catalytic routes and oxidation mechanisms in photoreforming of polyols, J. Catal. (2016), http://dx.doi.org/10.1016/j.jcat.2016.08.009

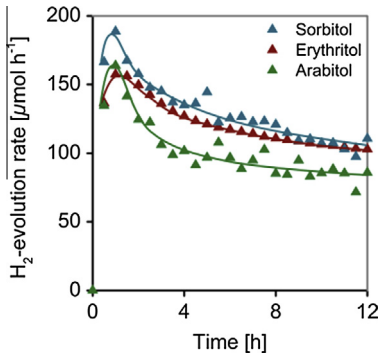

Fig. 6. Course of H_2-evolution rates during photoreforming of C_4–C_6 polyols. Reaction conditions: 75 mg photocatalyst, 100 mL aqueous oxygenate solution (20 mM), 288 K, 1 bar Ar, 300 W Xe-lamp (CM1).

polyol conversion must predominantly proceed through oxidative cleavage of an internal C–C bond, i.e. the C2–C3 bond in erythritol, arabitol, and sorbitol (Scheme 7, and SI-Schemes 1 and 2).

Constant selectivity profiles for C_{2+} aldoses over time indicate that every C–C bond may also undergo oxidative cleavage in the first step although the internal cleavage is preferred. Similar distributions of these aldoses were encountered in studies conducted over noble metal decorated TiO_2 [29,45]. However, we did not find evidence for the generation of gluconic acid as reported earlier [29,45].

C_n aldoses generated from oxidation of a terminal polyol carbon, i.e. erythrose from erythritol, arabinose and lyxose from arabitol, and glucose from sorbitol are present in small quantities (initial selectivities of 1–8% decreasing with increasing polyol carbon number). C_n ketoses resulting from oxidation of a secondary carbon in 2-position (i.e., formation of erythrulose from erythritol with an initial selectivity of 3%) are absent in the cases of arabitol and sorbitol photoreforming. These low selectivities to C_n ketoses and C_n aldoses from polyols corroborate the minor contribution of pathways yielding C_n species with primary or secondary sp^2-carbon.

Compounds bearing non-functionalized carbon as a consequence of dehydration reactions were not observed except for small quantities of acetaldehyde (e.g., of 30 μmol after 12 h during photoreforming of erythritol) that were present with all polyols and decreasing with increasing polyol chain length. The origin, properties and impact of multiple formic acid esters (summed to a total amount of "formates") encountered with minor abundance as a consequence of the presence of cyclic hemiacetal intermediates (erythrose, arabinose, xylose, lyxose and glucose) are currently under investigation.

Thus, initial anodic transformations of erythritol, arabitol and sorbitol involve multiple oxidative C–C-scission pathways. The reaction pathways for sorbitol photoreforming are exemplarily displayed in Scheme 7 (reaction pathways for erythritol and arabitol conversion are found in SI-Schemes 1 and 2). Generally, oxidative cleavage of each individual C–C bond is feasible in the first step. However, cleavage of the internal C–C bonds, i.e. C2–C3 for erythritol and arabitol and C2–C3 preferred over C3–C4 for sorbitol, constitutes the dominant reaction pathways.

3.4. Mechanistic aspects of anodic transformations of polyols

A unified description involving two different reaction sites is proposed to rationalize the elementary steps in the anodic transformations of polyols, i.e. oxidative C–C cleavage (direct charge carrier transfer), oxidation to the corresponding aldehydes and ketones (indirect charge carrier transfer) and dehydration (side reaction within indirect mechanism).

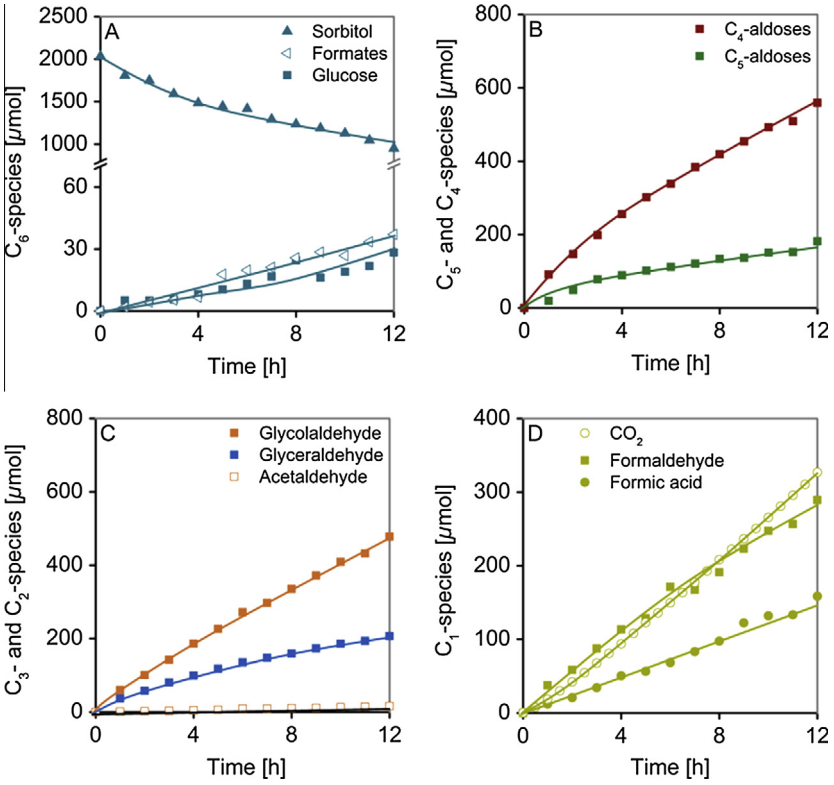

Fig. 7. Temporal profiles of anodic reaction products formed during sorbitol photoreforming. (A) Course of amount of sorbitol and C_6-intermediates. Course of (B) C_5/C_4-, (C) C_3-/C_2- and (D) C_1-species generated. Reaction conditions: 75 mg photocatalyst, 100 mL aqueous sorbitol solution (20 mM), 288 K, 1 bar Ar, 300 W Xe-lamp (CM1).

Please cite this article in press as: K.E. Sanwald et al., Catalytic routes and oxidation mechanisms in photoreforming of polyols, J. Catal. (2016), http://dx.doi.org/10.1016/j.jcat.2016.08.009

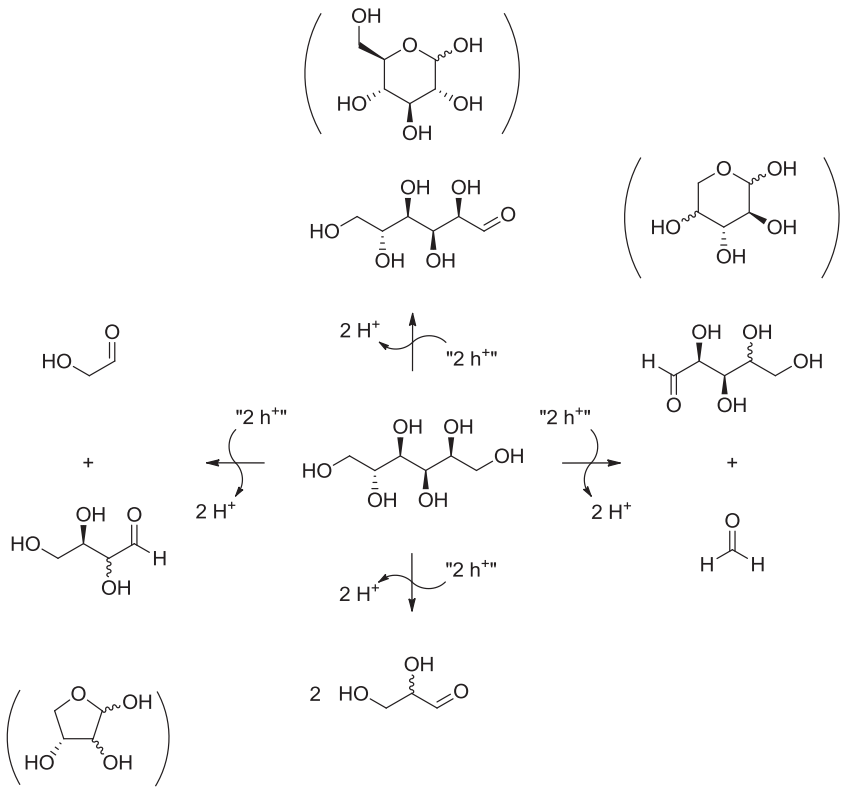

Scheme 7. Reaction network for photocatalytic reforming of sorbitol. Initial anodic conversion may proceed through four pathways. C–C-scission (C2–C3) to form glycolaldehyde and erythrose constitutes the dominant reaction pathway. Cleavage of all other C–C bonds and formation of glucose represent minor reaction channels.

Oxidative C–C cleavage is initialized by direct electron transfer from 'deep surface hole traps', which are constituted by chemisorbed oxygenates on terminal OH-groups at oxygen coordinatively unsaturated Ti-sites [18,31,46] as illustrated in Scheme 8, Sequence (1). As a consequence of hole transfer to the adsorbate, alkoxy radicals are formed which undergo β-C–C-scission [47] to form one aldehyde equivalent and a carbon-centered radical. Oxidation of the latter radicals to a second aldehyde moiety under anaerobic conditions is hypothesized to proceed preferentially through injection of an electron into the conduction band of TiO_2, i.e. a "current doubling" process. Formally, the reaction products from C–C-cleavage reflect the outcome of a Malaprade periodic acid oxidation chemistry [48].

Beyond that, holes may be trapped at surface lattice oxygen sites [Ti···O···Ti] [18,31,46]. These sites act as shallow hole traps that catalyze ·OH-radical/Fenton's reagent like chemical transformations (Scheme 8, Sequence (2)), i.e., the formation of the corresponding aldehydes and ketones from polyols [18,31]. Carbon-centered radicals from H-abstraction may form stable organic species upon current doubling (Scheme 8, sequence (3)). In a side reaction during photoreforming, the radicals may undergo an acid-catalyzed *ß*-shift (Scheme 8, sequence (3a)) which subsequently results in the associated dehydration products [18,49–51], e.g., production of HA from glycerol. Acid-catalyzed elimination of water upon *ß*-shift of a carbon-centered radical to form a carbon radical (or intermediate radical cation upon proton association) stabilized by a vicinal carbonyl group (Scheme 8) is well-known to occur during free OH-radical mediated oxidations [49–51].

Aerobic photooxidation studies demonstrated that the contributions of direct and indirect oxidation mechanisms critically depend on molecular reactant structure [46,52–54]. For instance, photocatalytic degradation of phenol over TiO_2 P 25 proceeded predominantly through interaction with 'shallowly trapped holes' with a minor contribution of a direct hole transfer mechanism [53]. Polyols possess a high tendency toward coordination to Ti (IV) cations. Evidence for a bidentate mode of binding was provided from the changes in the pre-edge structure in Ti K-edge XANES [55]. Those were interpreted in terms of an almost quantitative change in coordination environment around Ti(IV) sites from square pyramidal toward octahedral upon adsorption of polyols. In case of glycerol, IR-spectroscopic studies provide evidence that glycerol dissociatively establishes a bridging alkoxy bond *via* a primary OH-functionality to a coordinatively unsaturated Ti(IV) site [56,57]. An increasing tendency for polyol chemisorption with increasing number of OH-functionalities was shown for competitive adsorption of water and polyols on hydrated Al_2O_3 [56,58].

Our investigations into the anodic reaction networks of ethylene glycol [18] and C_3–C_6 polyols show a change from oxidation of a primary carbon (reaction of ethylene glycol to glycolaldehyde *via* an indirect mechanism) to C–C-cleavage (direct mechanism) for glycerol and higher polyols as the dominant reaction pathway. The relative contributions of direct and indirect mechanisms to the anodic conversion of C_n polyols are presented in Fig. 8 (Data for C_2-polyol was taken from Ref. [18]). The contributions were derived from the rate constants from kinetic modeling in case of ethylene glycol and glycerol and the initial selectivities of the primary products for C_4–C_6 polyol photoreforming. The direct mechanism becomes progressively dominant with increasing polyol chain length, i.e. the relative contribution increases from 15% for ethylene glycol to 61% for glycerol and 98% for sorbitol photoreforming, respectively. This is in line with the complexation of coordinatively unsaturated Ti(IV)-sites expected to be more effective, i.e. a larger polyol fraction in a chemisorbed state at constant concentration, with increasing number of anchoring OH-groups. In parallel, the participation of indirect reaction channels diminishes accordingly. The decreasing selectivity for dehydration with

Please cite this article in press as: K.E. Sanwald et al., Catalytic routes and oxidation mechanisms in photoreforming of polyols, J. Catal. (2016), http://dx.doi.org/10.1016/j.jcat.2016.08.009

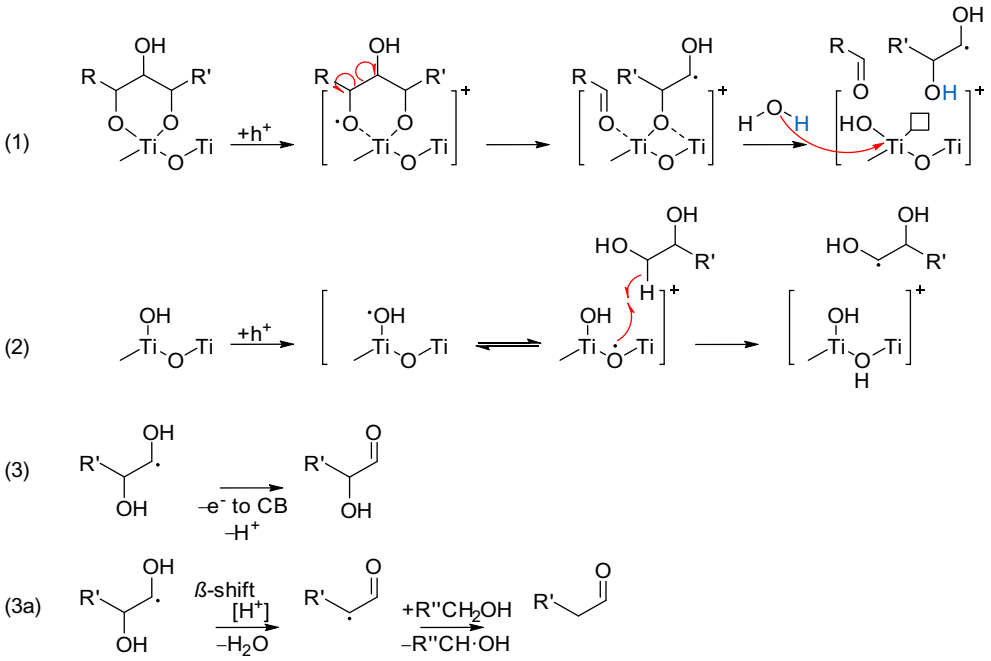

Scheme 8. Illustration of proposed anodic transformations via direct and indirect oxidation mechanisms. (1) Direct hole transfer to a chemisorbed oxygenate on coordinatively unsaturated Ti(IV)-OH site to generate an alkoxide radical followed by ß-C–C-scission. Nucleophilic attack of water is proposed for active site recovery and product release. (2) Generation of carbon centered H-loss radicals via interaction with shallowly trapped holes at surface lattice oxygen sites. (3) Formation of stable organic species through either current doubling of carbon-centered radicals or dehydration via acid-catalyzed ß-shift of the radicals.

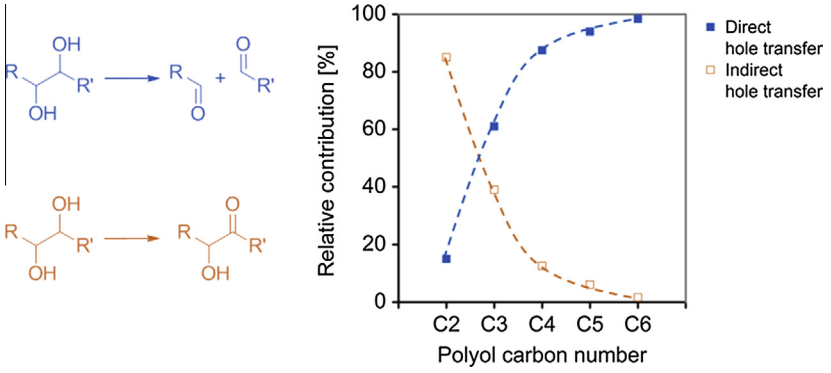

Fig. 8. Relative contributions of direct (C–C-cleavage) and indirect (oxidation to C_n aldoses and ketoses and dehydration) charge transfer mechanisms to the anodic transformations of C_2–C_6 polyols during photoreforming over Rh/TiO_2 derived from reaction pathway analysis. Data for C_2-polyol was taken from Ref. [18].

increasing polyol carbon number that leads to the absence of the respective products during photoreforming of C_4–C_6 polyols corroborates a side-reaction within the indirect mechanism.

4. Conclusions

Photocatalytic rates of linear C_1–C_3 oxygenates are primarily dependent on the substrate specific apparent adsorption constants and follow a Langmuir adsorption model. In the anodic half-reactions of photoreforming linear polyols are converted *via* (i) oxidative rupture of C–C bonds, (ii) oxidation to the corresponding aldoses or ketoses or (iii) light-driven dehydration, while evolving H_2 at the cathode. The first pathway is proposed to result from direct hole transfer to the chemisorbed oxygenate on terminal Ti (IV)-OH groups to form alkoxy-radicals which undergo *ß*-C–C-cleavage. The latter pathways are attributed to an indirect mechanism initiated by hole trapping at surface lattice oxygen sites [Ti···O···Ti].

Accordingly, the anodic reaction network of glycerol photoreforming follows four reaction pathways. Oxidative C–C-cleavage leads to glycolaldehyde and formaldehyde as the dominant pathway (61%). Oxidation of the primary or secondary carbon leads to glyceraldehyde (26%) or dihydroxyacetone (13%), respectively. Light-driven dehydration of glycerol to hydroxyacetone proceeds in a minor side-reaction. With increasing polyol chain length (number of carbons and OH-groups) the selectivities shift to favor anodic conversion through C–C-cleavage even further with internal C–C bonds preferentially cleaved over terminal ones. This is attributed to the increasing number of anchoring OH-functionalities favoring conversion through a direct hole transfer mechanism.

Acknowledgments

We would like to thank Clariant for fruitful discussions within the framework of MuniCat and the iC[4] PhotoCOO project. The authors are grateful to Donald M. Camaioni for critical reading of

the manuscript. Additionally, we would like to thank the German Federal Ministry of Education and Research (BMBF) for financial support (project no. 01RC1106A). K.E.S. gratefully acknowledges financial support by the Fond der Chemischen Industrie (FCI). The authors thank Xaver Hecht for BET and H_2-chemisorption measurements and Martin Neukamm for AAS measurements. Christine Schwarz and Martina Haack are acknowledged for technical assistance concerning NMR and HPLC analysis, respectively.

Appendix A. Supplementary material

Supplementary data associated with this article can be found, in the online version, at http://dx.doi.org/10.1016/j.jcat.2016.08.009.

References

[1] K. Shimura, H. Yoshida, Energy Environ. Sci. 4 (2011) 2467–2481.
[2] R.M. Navarro, M.C. Sanchez-Sanchez, M.C. Alvarez-Galvan, F.d. Valle, J.L.G. Fierro, Energy Environ. Sci. 2 (2009) 35–54.
[3] D. Kondarides, V. Daskalaki, A. Patsoura, X. Verykios, Catal. Lett. 122 (2008) 26–32.
[4] Y. Ma, X. Wang, Y. Jia, X. Chen, H. Han, C. Li, Chem. Rev. 114 (2014) 9987–10043.
[5] X. Chen, S. Shen, L. Guo, S.S. Mao, Chem. Rev. 110 (2010) 6503–6570.
[6] M. Cargnello, A. Gasparotto, V. Gombac, T. Montini, D. Barreca, P. Fornasiero, Eur. J. Inorg. Chem. 2011 (2011) 4309–4323.
[7] Z.H.N. Al-Azri, W.-T. Chen, A. Chan, V. Jovic, T. Ina, H. Idriss, G.I.N. Waterhouse, J. Catal. 329 (2015) 355–367.
[8] F. Dionigi, P.C.K. Vesborg, T. Pedersen, O. Hansen, S. Dahl, A. Xiong, K. Maeda, K. Domen, I. Chorkendorff, J. Catal. 292 (2012) 26–31.
[9] W. Jiao, L. Wang, G. Liu, G.Q. Lu, H.-M. Cheng, ACS Catal. 2 (2012) 1854–1859.
[10] J. Zhang, Q. Xu, Z. Feng, M. Li, C. Li, Angew. Chem. Int. Ed. 120 (2008) 1790–1793.
[11] Y.K. Kho, A. Iwase, W.Y. Teoh, L. Mädler, A. Kudo, R. Amal, J. Phys. Chem. C 114 (2010) 2821–2829.
[12] A. Tanaka, S. Sakaguchi, K. Hashimoto, H. Kominami, ACS Catal. 3 (2013) 79–85.
[13] A.J. Bard, M.A. Fox, Acc. Chem. Res. 28 (1995) 141–145.
[14] A.J. Bard, J. Photochem. 10 (1979) 59–75.
[15] J. Chen, D.F. Ollis, W.H. Rulkens, H. Bruning, Water Res. 33 (1999) 1173–1180.
[16] K. Lalitha, G. Sadanandam, V.D. Kumari, M. Subrahmanyam, B. Sreedhar, N.Y. Hebalkar, J. Phys. Chem. C 114 (2010) 22181–22189.
[17] P. Panagiotopoulou, E.E. Karamerou, D.I. Kondarides, Catal. Today 209 (2013) 91–98.
[18] T.F. Berto, K.E. Sanwald, W. Eisenreich, O.Y. Gutiérrez, J.A. Lercher, J. Catal. 338 (2016) 68–81.
[19] R. Chong, J. Li, X. Zhou, Y. Ma, J. Yang, L. Huang, H. Han, F. Zhang, C. Li, Chem. Commun. 50 (2014) 165–167.
[20] M. Murdoch, G.I.N. Waterhouse, M.A. Nadeem, J.B. Metson, M.A. Keane, R.F. Howe, J. Llorca, H. Idriss, Nat. Chem. 3 (2011) 489–492.
[21] R. Su, R. Tiruvalam, A.J. Logsdail, Q. He, C.A. Downing, M.T. Jensen, N. Dimitratos, L. Kesavan, P.P. Wells, R. Bechstein, ACS Nano 8 (2014) 3490–3497.
[22] W. Jones, R. Su, P.P. Wells, Y. Shen, N. Dimitratos, M. Bowker, D. Morgan, B.B. Iversen, A. Chutia, F. Besenbacher, G.J. Hutchings, PCCP 16 (2014) 26638–26644.
[23] Y. Hang Li, J. Xing, Z. Jia Chen, Z. Li, F. Tian, L. Rong Zheng, H. Feng Wang, P. Hu, H. Jun Zhao, H. Gui Yang, Nat. Commun. 4 (2013) 2500.
[24] H. Bahruji, M. Bowker, P.R. Davies, L.S. Al-Mazroai, A. Dickinson, J. Greaves, D. James, L. Millard, F. Pedrono, J. Photoch. Photobio. A 216 (2010) 115–118.
[25] H. Bahruji, M. Bowker, P.R. Davies, F. Pedrono, Appl. Catal. B 107 (2011) 205–209.
[26] G.N. Nomikos, P. Panagiotopoulou, D.I. Kondarides, X.E. Verykios, Appl. Catal. B 146 (2014) 249–257.
[27] X. Fu, J. Long, X. Wang, D.Y.C. Leung, Z. Ding, L. Wu, Z. Zhang, Z. Li, X. Fu, Int. J. Hydrogen Energy 33 (2008) 6484–6491.
[28] V.M. Daskalaki, D.I. Kondarides, Catal. Today 144 (2009) 75–80.
[29] R. Chong, J. Li, Y. Ma, B. Zhang, H. Han, C. Li, J. Catal. 314 (2014) 101–108.
[30] C. Minero, E. Pelizzetti, P. Pichat, M. Sega, M. Vincenti, Environ. Sci. Technol. 29 (1995) 2226–2234.
[31] C. Minero, A. Bedini, V. Maurino, Appl. Catal. B 128 (2012) 135–143.
[32] V. Maurino, A. Bedini, M. Minella, F. Rubertelli, E. Pelizzetti, C. Minero, J. Adv. Oxid. Technol. 11 (2008) 184–192.
[33] T. Montini, V. Gombac, L. Sordelli, J.J. Delgado, X. Chen, G. Adami, P. Fornasiero, ChemCatChem 3 (2011) 574–577.
[34] J. Schnaidt, M. Heinen, D. Denot, Z. Jusys, R.J. Behm, J. Electroanal. Chem. 661 (2011) 250–264.
[35] C.A. Martins, M.J. Giz, G.A. Camara, Electrochim. Acta 56 (2011) 4549–4553.
[36] Y. Kwon, K.J.P. Schouten, M.T.M. Koper, ChemCatChem 3 (2011) 1176–1185.
[37] H.J. Kim, J. Lee, S.K. Green, G.W. Huber, W.B. Kim, ChemSusChem 7 (2014) 1051–1056.
[38] L. Roquet, E.M. Belgsir, J.M. Léger, C. Lamy, Electrochim. Acta 39 (1994) 2387–2394.
[39] X. Fu, X. Wang, D.Y.C. Leung, Q. Gu, S. Chen, H. Huang, Appl. Catal. B 106 (2011) 681–688.
[40] A. Gallo, M. Marelli, R. Psaro, V. Gombac, T. Montini, P. Fornasiero, R. Pievo, V.D. Santo, Green Chem. 14 (2012) 330–333.
[41] T. Sakata, T. Kawai, Chem. Phys. Lett. 80 (1981) 341–344.
[42] T. Sakata, T. Kawai, K. Hashimoto, J. Phys. Chem.-US 88 (1984) 2344–2350.
[43] B. Kraeutler, A.J. Bard, J. Am. Chem. Soc. 100 (1978) 5985–5992.
[44] X.-J. Zheng, L.-F. Wei, Z.-H. Zhang, Q.-J. Jiang, Y.-J. Wei, B. Xie, M.-B. Wei, Int. J. Hydrogen Energy 34 (2009) 9033–9041.
[45] M. Bellardita, E.I. García-López, G. Marcì, L. Palmisano, Int. J. Hydrogen Energy 41 (2016) 5934–5947.
[46] J.F. Montoya, M.F. Atitar, D.W. Bahnemann, J. Peral, P. Salvador, J. Phys. Chem. C 118 (2014) 14276–14290.
[47] A. Boto, D. Hernández, R. Hernández, E. Suárez, J. Org. Chem. 68 (2003) 5310–5319.
[48] G. Dryhurst, Periodate Oxidation of Diol and Other Functional Groups: Analytical and Structural Applications, vol. 2, Pergamon Press, Oxford, 1970 (Chapter 2 and 3).
[49] A.L. Buley, R.O.C. Norman, R.J. Pritchett, J. Chem. Soc. B (1966) 849–852.
[50] C. Walling, R.A. Johnson, J. Am. Chem. Soc. 97 (1975) 2405–2407.
[51] D. Jiang, S. Barata-Vallejo, B.T. Golding, C. Ferreri, C. Chatgilialoglu, Org. Biomol. Chem. 10 (2012) 1102–1107.
[52] C. Minero, G. Mariella, V. Maurino, E. Pelizzetti, Langmuir 16 (2000) 2632–2641.
[53] C. Minero, G. Mariella, V. Maurino, D. Vione, E. Pelizzetti, Langmuir 16 (2000) 8964–8972.
[54] J.M. Kesselman, O. Weres, N.S. Lewis, M.R. Hoffmann, J. Phys. Chem. B 101 (1997) 2637–2643.
[55] I.A. Shkrob, M.C. Sauer, D. Gosztola, J. Phys. Chem. B 108 (2004) 12512–12517.
[56] J.R. Copeland, X.-R. Shi, D.S. Sholl, C. Sievers, Langmuir 29 (2013) 581–593.
[57] J.R. Copeland, I.A. Santillan, S.M. Schimming, J.L. Ewbank, C. Sievers, J. Phys. Chem. C 117 (2013) 21413–21425.
[58] W. van Bronswijk, H.R. Watling, Z. Yu, Colloid. Surface A 157 (1999) 85–94.